Geosci. Model Dev. Discuss., doi:10.5194/gmd-2017-82, 2017
Manuscript under review for journal Geosci. Model Dev.
Discussion started: 20 April 2017

Geoscientific Model Development Discussions

^{231}Pa and ^{230}Th in the ocean model of the Community Earth System Model (CESM1.3)

Sifan Gu[1], Zhengyu Liu[1]

[1]Department of Atmospheric and Oceanic Sciences and Center for Climate Research, University of Wisconsin-Madison, Madison, WI, USA

Correspondence to: Sifan Gu (sgu28@wisc.edu)

Abstract

Sediment ^{231}Pa/^{230}Th activity ratio is emerging as an important proxy for deep ocean circulation in the past. In order to allow for a direct model-data comparison and to improve our understanding of sediment ^{231}Pa/^{230}Th activity ratio, we implement ^{231}Pa and ^{230}Th in the ocean component of the Community Earth System Model (CESM). In addition to the biotic ^{231}Pa and ^{230}Th that is fully coupled with the active marine ecosystem module, another form of abiotic ^{231}Pa and ^{230}Th have also been implemented with prescribed particle flux fields of the present climate. The comparison of the two forms of ^{231}Pa and ^{230}Th helps to isolate the influence of the particle fluxes from that of circulation. Under present day climate forcing, our model is able to simulate water column ^{231}Pa and ^{230}Th activity and sediment ^{231}Pa/^{230}Th activity ratio in good agreement with available observations. For past climate, our model is able to simulate a comparable magnitude of the change of sediment ^{231}Pa/^{230}Th activity ratio between the state with and without active AMOC in reconstruction. In addition, in hosing experiments, the biotic and abiotic sediment ^{231}Pa/^{230}Th activity ratios behave similarly over large areas of low productivity, but can differ substantially in some regions of high productivity, indicating the importance of biological productivity in addition to physical circulation. Therefore, our model provides a potentially powerful tool to help our interpretation of sediment ^{231}Pa/^{230}Th reconstructions and to improve our understanding of past ocean circulation and climate changes.

1. Introduction

Sediment $^{231}Pa/^{230}Th$ activity ratio has been used as a proxy to reconstruct ocean circulation in the past (e.g. Yu et al. 1996; McManus et al. 2004; Gherardi et al. 2009). ^{231}Pa (32.5 ka half-life) and ^{230}Th (75.2 ka half-life) are produced at a constant rate approximately uniformly in the ocean by the α decay of ^{235}U and ^{234}U, respectively, with a production activity ratio of 0.093 (Henderson and Anderson, 2003). Water column ^{231}Pa and ^{230}Th are subject to particle scavenging and transport to sediments (Bacon and Anderson, 1982; Nozaki et al., 1987). Differential scavenging efficiency results in different ocean residence time: ^{231}Pa has a residence time of approximately 111 years and ^{230}Th has a residence time of approximately 26 years (Yu et al., 1996). Longer residence time of ^{231}Pa than ^{230}Th makes ^{231}Pa more subject to ocean transport and therefore in modern ocean about 45% of ^{231}Pa produced in the Atlantic is transported to the Southern Ocean (Yu et al., 1996), resulting a lower than 0.093 sediment $^{231}Pa/^{230}Th$ activity ratio in the North Atlantic and higher than 0.093 sediment $^{231}Pa/^{230}Th$ activity ratio in the Southern Ocean.

The application of the principle above to interpret sediment $^{231}Pa/^{230}Th$ as the strength of overturning circulation, however, can be complicated by other factors, leading to uncertainties in using $^{231}Pa/^{230}Th$ as a tracer for paleocirculation (Keigwin and Boyle, 2008; Lippold et al., 2009; Scholten et al., 2008). In addition to ocean transport, sediment $^{231}Pa/^{230}Th$ is also influenced by particle flux and composition (Chase et al., 2002; Geibert and Usbeck, 2004; Scholten et al., 2008; Siddall et al., 2007; Walter et al., 1997). The region of a higher particle flux tends to have a higher $^{231}Pa/^{230}Th$ (Kumar et al., 1993; Yong Lao et al., 1992), which is referred to as the "particle flux effect" (Siddall et al., 2005). High particle flux in the water column in a region will favor the removal of isotopes into the sediment, which leads to more isotopes transported into this region due to the down-gradient diffusive flux into this region and subsequently more removal of isotopes into the sediment. Since ^{231}Pa has a longer residence time, this effect is more prominent on ^{231}Pa than on ^{230}Th and therefore sediment $^{231}Pa/^{230}Th$ will be higher in high productivity regions. Also, opal is able to scavenge ^{231}Pa much more effectively than

^{230}Th, leading to higher ^{231}Pa/^{230}Th in high opal flux regions such as the Southern Ocean (Chase et al., 2002). Moreover, sediment ^{231}Pa/^{230}Th is suggested to record circulation change only within 1000 m above the sediment, instead of the whole water column, complicating the interpretation of sediment ^{231}Pa/^{230}Th reconstructions (Thomas et al., 2006). For example, sediment ^{231}Pa/^{230}Th approaching 0.093 during Heinrich Stadial event 1(HS1) from the subtropical North Atlantic is interpreted as the collapse of the Atlantic Meridional Overturning Circulation (AMOC) (McManus et al., 2004). If sediment ^{231}Pa/^{230}Th only records deepest water mass, it is possible that during HS1, AMOC shoals, as opposed to fully collapse, yet an increase of deep water imported from the Southern Ocean featuring high ^{231}Pa/$^{230\mathrm{Th}}$ can increase the sediment ^{231}Pa/^{230}Th approaching the production ratio (0.093) (Thomas et al., 2006). All these suggest the importance of incorporating ^{231}Pa and ^{230}Th into climate models for a direct model-data comparison for a thorough understanding of sediment ^{231}Pa/^{230}Th as well as past ocean circulation.

^{231}Pa and ^{230}Th have been simulated in previous modeling studies (Dutay et al., 2009; Henderson et al., 1999; Marchal et al., 2000; Siddall et al., 2005). Here we follow the scheme of Siddall et al., (2005) to implement ^{231}Pa and ^{230}Th into the Community Earth System Model (CESM). Siddall et al., (2005) uses prescribed particle fluxes. Our model ^{231}Pa and ^{230}Th are coupled to a marine ecosystem model (biotic) and therefore can be used to study the impact of ecosystem change on ^{231}Pa and ^{230}Th directly. To help to understand the influence of the particle flux, we have also implemented an abiotic version of ^{231}Pa and ^{230}Th, for which the particle fluxes are prescribed. By comparing the abiotic ^{231}Pa and ^{230}Th with the biotic ^{231}Pa and ^{230}Th, we will be able to separate the effect of circulation change from particle field change. In addition, the abiotic ^{231}Pa and ^{230}Th can be run without the marine ecosystem module, reducing computational cost by a factor of 3 in the ocean-alone model simulation and therefore making it a computationally efficient tracer for sensitivity studies.

This paper describes the details of ^{231}Pa and ^{230}Th in CESM and serves as a reference for future studies using this tracer module. In section 2, we describe the model and the implementation of ^{231}Pa and ^{230}Th. In sections 3, we describe the experimental design. We will finally compare simulated ^{231}Pa and ^{230}Th fields with observations, show model sensitivities on the parameter and also sediment $^{231}Pa/^{230}Th$ ratio response to freshwater forcing in Section 4.

2. Model Description

2.1 Physical Ocean Model

We implement ^{231}Pa and ^{230}Th in the ocean model (Parallel Ocean Program version 2, POP2) (Danabasoglu et al., 2012) of CESM (Hurrell et al., 2013). CESM is a state-of-the-art coupled climate model and studies describing model components and analyzing results can be found in a special collection in Journal of Climate (http://journals.ametsoc.org/topic/ccsm4-cesm1). We run the ocean-alone model, which is coupled to data atmosphere, land, ice and river runoff under the normal year forcing of CORE-II data (Large and Yeager, 2008), using the low-resolution version of POP2 with a nominal 3° horizontal resolution and 60 vertical layers.

2.2 Biogeochemical component (BGC)

POP2 has incorporated a marine ecosystem module that simulates biological variables (Moore et al., 2013). The marine ecosystem module has been validated against present day observations extensively (Doney et al., 2009; Long et al., 2013; Moore and Braucher, 2008; Moore et al., 2002, 2004). The implementation of ^{231}Pa and ^{230}Th requires four particle fields: $CaCO_3$, opal, particulate organic carbon (POC) and dust. These particle fields can be obtained from the ecosystem driver from the ecosystem module (Jahn et al., 2015). The ecosystem module simulates the particle fluxes in reasonable agreement with the present day observations. The pattern and magnitude of the annual mean particle fluxes ($CaCO_3$, opal, POC) leaving the euphotic zone at 105m are similar to the satellite observations (Fig. 7.2.5 and 9.2.2 in Sarmiento and Gruber 2006) (Fig. 1 a~c): particle fluxes are higher in the high productivity regions such as high latitudes and equatorial Pacific; opal flux is high in the Southern Ocean. For ocean-alone experiments, atmospheric dust deposition to the surface ocean is prescribed from Luo et al. (2003) (Fig. 1d).

Geosci. Model Dev. Discuss., doi:10.5194/gmd-2017-82, 2017
Manuscript under review for journal Geosci. Model Dev.
Discussion started: 20 April 2017

2.3 ^{231}Pa and ^{230}Th implementation

Two forms of ^{231}Pa and ^{230}Th are implemented in POP2: abiotic and biotic. Abiotic ^{231}Pa and ^{230}Th use particle fluxes prescribed as annual mean particle fluxes from the CESM marine ecosystem module under present day climate forcing (Fig.1). Biotic ^{231}Pa and ^{230}Th use particle fluxes computed simultaneously from the marine ecosystem module. Abiotic and biotic ^{231}Pa and ^{230}Th can be turned on at the case build time and the biotic ^{231}Pa and ^{230}Th requires the ecosystem module turned on at the same time.

The implementation of ^{231}Pa and ^{230}Th is based on Siddall et al., (2005) (Eq.(3)). ^{231}Pa and ^{230}Th are produced from the α decay of ^{235}U and ^{234}U uniformly everywhere at constant rate β^i ($\beta^{Pa} = 2.33*10^{-3}$ dpm m^{-3} yr^{-1}, $\beta^{Th} = 2.52*10^{-2}$ dpm m^{-3} yr^{-1}). ^{231}Pa and ^{230}Th are subjective to radioactive decay with the decay constant of λ^i ($\lambda^{Pa} = 2.13*10^{-5}$ yr^{-1}, $\lambda^{Th} = 9.22*10^{-6}$ yr^{-1}). In addition to ocean transport, which includes advection, convection, and diffusion, another important process contributes to ^{231}Pa and ^{230}Th activity is the reversible scavenging (term $w_S \frac{\partial A_p^i}{\partial z}$ *in Eq.*(3)) by sinking particles with a sinking velocity w_s, which describes the adsorption of isotopes onto sinking particles and desorption after the dissolution of particles (Detailed vertical differentiation scheme to calculate this term in the model is in the supplementary material). This process transports ^{231}Pa and ^{230}Th downward and leads to a general increase of ^{231}Pa and ^{230}Th activity with depth. We don't differentiate between particle sizes as in Dutay et al., (2009) and consider all particles as slowly sinking small particles with sinking velocity of w_s =1000 m yr^{-1} (Arsouze et al., 2009; Dutay et al., 2009; Kriest, 2002). The reversible scavenging considers total isotope activity (A_t^i) as two categories: dissolved isotopes (A_d^i) and particulate isotopes (A_p^i) (superscript i=1 and 2 refers to ^{231}Pa and ^{230Th}, respectively) as in Eq. (1) and assumes these two phases are in equilibrium, which is a reasonable assumption in the open ocean (Bacon and Anderson, 1982; Henderson et al., 1999; Moore and Hunter, 1985; Roy-Barman et al., 1996). Any particulate isotopes at the ocean bottom layer are removed from the

Geosci. Model Dev. Discuss., doi:10.5194/gmd-2017-82, 2017
Manuscript under review for journal Geosci. Model Dev.
Discussion started: 20 April 2017

Geoscientific Model Development Discussions
Open Access

ocean as sediment. The ratio between the particulate isotope activity and the dissolved isotope activity is set by a partition coefficient, K (Eq. (2)), where C_j is the ratio of particle concentration to the density of seawater (1024.5 kg m^{-3}). Subscript j refers to different particle types ($CaCO_3$, opal, POC and dust). The reversible scavenging scheme applied here is the same as the neodymium implementation in POP2 (Gu et al., 2017).

$$A_t^i = A_d^i + A_p^i \quad (1)$$

$$K_j^i = \frac{A_{j,p}^i}{A_{j,d}^i C_j} \quad (2)$$

Therefore, the conservation equation for ^{231}Pa and ^{230}Th activity can be written as

$$\frac{\partial A_t^i}{\partial t} = \beta^i - \lambda^i A_t^i - w_s \frac{\partial A_p^i}{\partial z} + Transport \quad (3)$$

where A_p^i can be calculated from Eq. (4) below by combining Eq. (1) and Eq. (2).

$$A_p^i = A_t^i \cdot \left(1 - \frac{1}{1 + K_{POC}^i \cdot R_{POC} + K_{CaCO_3}^i \cdot R_{CaCO_3} + K_{opal}^i \cdot R_{opal} + K_{dust}^i \cdot R_{dust}}\right) \quad (4)$$

3. Experiments

We run a control experiment (CTRL) and two experiments with different partition coefficients to show model sensitivity. We have both abiotic and biotic ^{231}Pa and ^{230}Th in CTRL, but only show abiotic ^{231}Pa and ^{230}Th in sensitivity experiments. Equilibrium partition coefficients for ^{231}Pa and ^{230}Th vary among different particle types and the magnitude of the partition coefficients for different particle types remains uncertain (Chase and Robert F, 2004; Chase et al., 2002; Luo and Ku, 1999). Since the control experiment in Siddall et al., (2005) is able to simulate major features of ^{231}Pa and ^{230}Th distributions, we use the partition coefficients from the control experiment in Siddall et al., (2005) in our CTRL (Table

Geosci. Model Dev. Discuss., doi:10.5194/gmd-2017-82, 2017
Manuscript under review for journal Geosci. Model Dev.
Discussion started: 20 April 2017

1). Two sensitivity experiments are performed with decreased (EXP_1) and increased (EXP_2) partition coefficients by a factor of 5 (Table 1).

All the experiments are ocean-alone experiments with the normal year forcing by CORE-II data (Large and Yeager, 2008). The ^{231}Pa and ^{230}Th activities are initiated from 0 in CTRL and are integrated for 2,000 model years until equilibrium is reached. EXP_1 and EXP_2 are initiated from 1,400 model year of CTRL and are integrated for another 800 model years to reach equilibrium.

To test how sediment ^{231}Pa/^{230}Th ratio responds to the change of AMOC, we carried out a fresh water perturbation experiment (HOSING) with both abiotic and biotic ^{231}Pa and ^{230}Th. Starting from 2,000 model year of CTRL, a freshwater flux of 1 Sv is imposed over the North Atlantic region of 50°N~70°N and the experiment is integrated for 1400 model years until both abiotic and biotic sediment ^{231}Pa/^{230}Th ratio have reached quasi-equilibrium. The partition coefficients used in HOSING are the same as in CTRL.

4. Results

4.1 Control Experiment

Abiotic and biotic version of ^{231}Pa and ^{230}Th in CTRL show identical results. Abiotic and biotic dissolved and particulate ^{231}Pa and ^{230}Th in CTRL are highly correlated with each other (Fig. 2e-h) with correlations larger than 0.995 and regression coefficients are all near 1.0 (R^2>0.995) (Fig. 2e-h). The correlation coefficient between abiotic and biotic sediment ^{231}Pa/^{230}Th activity ratios in CTRL is 0.99 (N=7879 points) and the regression coefficient between them is 0.9 (R^2=0.98) (Fig. 4a). This is expected because the particle fields used in abiotic version are the climatology of the particle fields used in the biotic version for the present day. Therefore, under the same climate forcing, abiotic and biotic version of ^{231}Pa and ^{230}Th should be very similar. For the discussion of results in CTRL below, we only discuss the abiotic ^{231}Pa and ^{230}Th.

The residence time of both ^{231}Pa and ^{230}Th in CTRL are comparable with observations. Residence time in CTRL is 118 yr for ^{231}Pa and 33 yr for ^{230}Th (Table

1), which are of the same magnitude as 111 yr for ^{231}Pa and 26 yr for ^{230}Th in observation (Yu et al., 1996).

CTRL can simulate the general features of the water column ^{231}Pa and ^{230}Th activities. Both dissolved and particulate activities for ^{231}Pa and ^{230}Th increase with depth in CTRL except in the regions of deep water formation, as shown in the zonal mean Atlantic dissolved and particulate ^{231}Pa and ^{230}Th activities (Fig. 2a-d). The dissolved and particulate ^{231}Pa and ^{230}Th activities are also at the same order of magnitude as in observations (Colley et al., 1995; Luo et al., 2010; Mangini and Key, 1983; Moran et al., 1997, 2002; Rutgers van der Loeff and Berger, 1993; VOGLER et al., 1998; Walter et al., 1997). Our CTRL shows similar results as in Siddall et al., (2005) (their Fig. 2). The patterns of dissolved ^{231}Pa and ^{230}Th activities are similar except in the Southern Ocean, where high opal flux effectively removes ^{231}Pa to sediment.

A more quantitative model-data comparison is shown in Fig. 3. The correlation between model and observations are significant at 0.01 confidence level for all dissolved and particulate ^{231}Pa and ^{230}Th: $[^{231}Pa]_d$ correlation is 0.65, $[^{230}Th]_d$ correlation is 0.73, $[^{231}Pa]_p$ correlation is 0.33 and $[^{230}Th]_p$ correlation is 0.62. The linear regression coefficient, an indication of model ability to simulate ^{231}Pa and ^{230}Th activity (Dutay et al., 2009), is near 1.0 for dissolved ^{231}Pa and ^{230}Th (1.14 for $[^{231}Pa]_d$ and 1.04 for $[^{230}Th]_d$), suggesting that CTRL can simulate the dissolved ^{231}Pa and ^{230}Th in good agreement with observations. However, the simulation of the particulate activity is not as good as the dissolved activity. Particulate activity is overall somewhat smaller than observations in the surface ocean and larger than observation in the deep ocean for both dissolved ^{231}Pa and ^{230}Th. The regression coefficient for particulate ^{231}Pa and ^{230}Th is 0.14 for $[^{231}Pa]_p$ and 0.42 for $[^{230}Th]_p$ (Fig. 3). This is also similar in previous modeling studies (Dutay et al., 2009; Siddall et al., 2005). One may think the performance of simulating $[^{231}Pa]_p$ and $[^{230}Th]_p$ can be improved by tuning model parameter: partition coefficient k. However, under current modeling scheme, changing partition coefficient k will have limited influenced on $[^{231}Pa]_p$ and $[^{230}Th]_p$, which will be discussed in section 4.2.

The sediment $^{231}Pa/^{230}Th$ activity ratios in CTRL is overall consistent with observations (Anderson et al., 1983, 1990, 1994; Bacon and Rosholt, 1982; Francois et al., 1993; Frank, 1996; Frank et al., 1994; Ku et al., 1972; Müller and Mangini, 1980; Schmitz et al., 1986; Scholten et al., 1995; Shimmield and Price, 1988; Shimmield et al., 1986; Walter et al., 1997; Yang et al., 1986; Yong Lao et al., 1992; Yong-Liang Yang et al., 1995; Yu et al., 1996). The North Atlantic shows low sediment $^{231}Pa/^{230}Th$ activity ratio as in observations because ^{231}Pa is more subject to transport to the Southern Ocean by active ocean circulation than ^{230}Th. The Southern Ocean maximum in the sediment $^{231}Pa/^{230}Th$ activity ratio is also simulated in CTRL, which is caused by high opal fluxes in the Southern Ocean preferentially removes ^{231}Pa into sediment ($K_{opal}^{231Pa} > K_{opal}^{230Th}$), as well as upwelling in the Southern Ocean brings up deep water enriched with ^{231}Pa, which is transported from the North Atlantic, to shallower depth and further contribute to the scavenging. CTRL can also produce higher sediment $^{231}Pa/^{230}Th$ activity ratio in regions with high particle production (e.g. the Eastern equatorial Pacific, the North Pacific and the Indian Ocean) due to the "particle flux effect". However, this particle flux effect is less effective in the North Atlantic than in the North Pacific and the Indian Ocean due to active deep ocean circulation transporting ^{231}Pa southward in the Atlantic (Yu et al., 1996).

4.2 Sensitivity on partition coefficient K

In this section, we show model sensitivity on partition coefficient by increasing and decreasing the partition coefficient, K, by a factor of 5, but keep the relative ratio for different particles the same (Table 1). Our model shows similar sensitivity to that in Siddall et al., (2005) as discussed below.

Increasing K will decrease water column dissolved ^{231}Pa and ^{230}Th activities but won't change particulate ^{231}Pa and ^{230}Th too much (Fig. 5). Larger K will lead to more ^{231}Pa and ^{230}Th attached to particles and further buried into sediment, which increases the sink for the ^{231}Pa and ^{230}Th budget. With the sources for ^{231}Pa and ^{230}Th staying the same, dissolved ^{231}Pa and ^{230}Th will be reduced. Increasing K will

Geosci. Model Dev. Discuss., doi:10.5194/gmd-2017-82, 2017
Manuscript under review for journal Geosci. Model Dev.
Discussion started: 20 April 2017

also reduce the vertical gradient of dissolved ^{231}Pa and ^{230}Th as reversible scavenging act as the vertical transport and increase this vertical transport can decrease the vertical gradient. However, change in the particulate ^{231}Pa and ^{230}Th is small. As stated in Siddall et al., (2005), if we neglect the transport term and the decay term in Eq. (3) and assume particulate phase activity at the surface as 0, when reach equilibrium, the activity of particulate phase will be as in Eq. (5). The particulate phase activity only depends on the production rate, the particle settling velocity and depth. The particulate phase activity will increase linearly with depth and any departure from this linear relationship with depth is due to ocean transport, which is suggested by observations (Bacon and Anderson, 1982; Roy-Barman et al., 1996). Therefore, changing K will have limited influence on particulate phase activity.

$$A_p^i(z) = \frac{\beta^i}{w_s} \cdot z \qquad (5)$$

Increasing K will also reduce the spatial gradient in sediment ^{231}Pa/^{230}Th activity ratio and vice versa (Fig. 6). Larger K will decrease the ^{231}Pa and ^{230}Th residence time and most isotopes produced in the water column are removed into sediment locally (Table 1). Therefore, sediment ^{231}Pa/^{230}Th ratio becomes more homogeneous and approaching the production ration of 0.093 (Fig. 6b). The sediment ^{231}Pa/^{230}Th activity ratio in EXP_1 and EXP_2 departures from observations significantly, suggesting the partition coefficient in CTRL is of the right magnitude.

4.3. Sediment ^{231}Pa/^{230}Th ratio in HOSING

With the AMOC collapsing, the ^{231}Pa/^{230}Th ratio tends to increase over most of the North Atlantic, consistent with paleo proxy evidence there. In HOSING, after applying extra freshwater to the North Atlantic, AMOC strength quickly decreases to a minimum of 2 Sv at around year 300 (AMOC_off)(Fig. 7a). During the AMOC_off state, compared with CTRL of active AMOC (AMOC_on), both abiotic and biotic sediment $^{231}Pa/^{230}Th$ ratio shows an overall increase in the North Atlantic and a decrease in the South Atlantic (Fig. 8b and d) because of the reduced southward transport of ^{231}Pa from the North Atlantic by AMOC. In most area of the Atlantic, the evolution of abiotic and biotic sediment $^{231}Pa/^{230}Th$ activity ratio in HOSING are highly correlated (Fig. 9a). The change of sediment $^{231}Pa/^{230}Th$ ratio from AMOC_on to AMOC_off are similar in abotic and biotic version (Fig.9b). The correlation between abiotic and biotic sediment $^{231}Pa/^{230}Th$ ratio change is 0.72 (1455points) and the linear regression coefficient is 0.71 (R^2 = 0.52). This suggests that abiotic sediment $^{231}Pa/^{230}Th$ activity ratio can capture the major feature of biotic $^{231}Pa/^{230}Th$ activity ratio in our model and also circulation effect on sediment $^{231}Pa/^{230}Th$ activity ratio is more dominant than the biological effect in HOSING. The pattern of abiotic (Fig.8a) sediment $^{231}Pa/^{230}Th$ ratio in the Atlantic in AMOC_off state is similar to the opal distribution (Fig.1b) because, without active circulation, sediment $^{231}Pa/^{230}Th$ ratio is more controlled by particle flux effect, which is similar to the case in the Pacific in CTRL. The overall increase of sediment $^{231}Pa/^{230}Th$ ratio in the North Atlantic in response to AMOC collapse can be seen more clearly in the time evolution of the sediment $^{231}Pa/^{230}Th$ ratio averaged from 20°N to 60°N in the North Atlantic in both the abiotic and biotic $^{231}Pa/^{230}Th$ (Fig.7b). Quantitatively, the $^{231}Pa/^{230}Th$ increases from 0.074 (0.074) in AMOC_on to 0.098 (0.095) in AMOC_off in the abiotic (biotic) version (Fig. 7b). Both abiotic and biotic version show average sediment $^{231}Pa/^{230}Th$ ratio in the North Atlantic near the production ratio of 0.093. This increase of $^{231}Pa/^{230}Th$ in both abiotic and biotic versions is also seen in the subtropical North Atlantic from the two sites near Bermuda Rise (Fig. 7e and f), which is, of comparable magnitude with the change from LGM to HS1 in reconstructions there (McManus et al., 2004). It is further noted that our abiotic sediment $^{231}Pa/^{230}Th$ ratio in HOSING behaves similarly to that in Siddall et al., (2007).

In spite of large scale patterns of sediment $^{231}Pa/^{230}Th$ ratio response, the magnitude of the change between AMOC_on and AMOC_off varies with location in both abiotic and biotic version because of the distribution of particle flux (Fig.7 and 8). Take the abiotic version as an example, the maximum increase in sediment

$^{231}Pa/^{230}Th$ ratio occurs near 40°N western Atlantic, where the opal production in our model is maximum (Fig. 1b). The sediment $^{231}Pa/^{230}Th$ ratio in this region in AMOC_on is larger than production ratio of 0.093 because particle flux effect due to the opal maximum provides extra ^{231}Pa to this region, which overwhelms the active ocean circulation transporting ^{231}Pa southward outside this region. Therefore, sediment $^{231}Pa/^{230}Th$ ratio in this region gets even larger (e.g. Fig. 7d). In AMOC_off, without active ocean circulation, the particle flux effect becomes more prominent because less ^{231}Pa is transported out of the North Atlantic.

The responses of abiotic and biotic sediment $^{231}Pa/^{230}Th$ ratio to the collapse of AMOC show similar behavior over most ocean region of low productivity but can differ significantly in high productivity region because of the change of productivity. Productivity in North Atlantic is suggested to be halved during AMOC collapse because of increased stratification, which reduces nutrient supply from deep ocean (Schmittner, 2005). In the CESM, the productivity in mid-latitude North Atlantic is indeed greatly reduced after the freshwater forcing. For example, at year 100 in HOSING, opal production from 30°N-50°N in the Atlantic is reduced by 50%~90% of its original value in CTRL (not shown). Therefore, in the first 100 years in HOSING, most biotic sediment $^{231}Pa/^{230}Th$ ratio show an initial decrease in the North Atlantic from the subtropics to the mid-latitude (Fig.7 d, e, and f, red dash). In the subpolar region, the productivity is increased in the model, leading to an initial increase of biotic sediment $^{231}Pa/^{230}Th$ ratio (Fig.7c). Furthermore, the detailed pattern of the difference between AMOC_off and AMOC_on in sediment $^{231}Pa/^{230}Th$ ratio is different. For example, the region (near 40°N west Atlantic), which has the maximum increase from AMOC_on to AMOC_off in abiotic sediment $^{231}Pa/^{230}Th$ ratio discussed above, shows a decrease in biotic sediment $^{231}Pa/^{230}Th$ ratio (Fig. 7d and Fig.8d) because there is no more opal maximum in this region in AMOC_off. A detailed discussion of the difference between abiotic and biotic sediment $^{231}Pa/^{230}Th$ ratio in different regions is beyond the scope of this paper. Overall, our model is able to simulate the correct magnitude of the sediment $^{231}Pa/^{230}Th$ ratio response to the change of AMOC, although the detailed difference between abiotic and biotic sediment $^{231}Pa/^{230}Th$ ratio response to fresh water forcing in different locations can be complicated.

5. Summary

^{231}Pa and ^{230}Th have been implemented into the ocean model of the CESM in both the biotic and abiotic forms. Our control experiment under present day climate forcing is able to simulate both ^{231}Pa and ^{230}Th water column activity and sediment $^{231}Pa/^{230}Th$ activity ratio consistent with observations by using the parameters that are suggested by Chase et al., (2002) and used in Siddall et al. (2005). Our sensitivity experiments with varying parameters suggest that these parameters are of the right magnitude. Furthermore, our model is able to simulate the overall sediment $^{231}Pa/^{230}Th$ ratio change in the North Atlantic with a magnitude comparable to the reconstruction in response to the collapse of AMOC, although the detailed regional response can be complicated in different regions. Finally, the abiotic form is able to capture many major features of that of the biotic form over large ocean areas, although the two forms can also differ significantly in some regions, especially the region with large productivity. Therefore, with both abiotic and biotic ^{231}Pa and ^{230}Th, our model can serve as a useful tool to improve our understanding of the processes of ^{231}Pa and ^{230}Th and also interpretations of sediment $^{231}Pa/^{230}Th$ reconstructions for past ocean circulation and climate changes.

Code availability:

The Nd isotope source code of both abiotic Nd and biotic Nd for CESM1.3 is included as supplementary material here.

Acknowledgement:

This work is supported by US NSF P2C2 projects NSF1401778 and NSF1401802, DOE DE-SC0006744 and the National Science Foundation of China No. 41130105. Computing resources (ark:/85065/d7wd3xhc) were provided by the Climate

Geoscientific Model Development Discussions

Simulation Laboratory at NCAR's Computational and Information Systems Laboratory, sponsored by the National Science Foundation and other agencies.

References:

Anderson, R. F., Bacon, M. P. and Brewer, P. G.: Removal of230Th and231Pa from the open ocean, Earth Planet. Sci. Lett., 62(1), 7–23, doi:10.1016/0012-821X(83)90067-5, 1983.

Anderson, R. F., Lao, Y., Broecker, W. S., Trumbore, S. E., Hofmann, H. J. and Wolfli, W.: Boundary scavenging in the Pacific Ocean: A comparison of 10Be and 231Pa, Earth Planet. Sci. Lett., 96(3-4), 287–304, doi:10.1016/j.cognition.2008.05.007, 1990.

Anderson, R. F., Fleisher, M. Q., Biscaye, P. E., Kumar, N., Dittrich, B., Kubik, P. and Suter, M.: Anomalous boundary scavenging in the Middle Atlantic Bight: evidence from 230Th, 231Pa, 10Be and 210Pb, Deep. Res. Part II, 41(2-3), 537–561, doi:10.1016/0967-0645(94)90034-5, 1994.

Arsouze, T., Dutay, J.-C., Lacan, F. and Jeandel, C.: Reconstructing the Nd oceanic cycle using a coupled dynamical – biogeochemical model, Biogeosciences, 6(12), 2829–2846, doi:10.5194/bg-6-2829-2009, 2009.

Bacon, M. and Anderson, R.: Distribution of Thorium Isotopes between dissolved and particulate forms in the deep sea, J. Geophys. Res. ..., 87(1), 2045–2056, 1982.
Bacon, M. P. and Rosholt, J. N.: Accumulation rates of 230Th, 231Pa, and some transition metals on the Bermuda Rise, Geochim. Cosmochim. Acta, 46, 651–666, 1982.

Chase, Z. and Robert F, A.: Comment on "On the importance of opal, carbonate, and lithogenic clays in scavenging and fractionating 230Th, 231Pa and 10Be in the ocean" by S. Luo and T.-L. Ku, Earth Planet. Sci. Lett., 220(1-2), 201–211, doi:10.1016/S0012-821X(04)00027-5, 2004.

Chase, Z., Anderson, R. F., Fleisher, M. Q. and Kubik, P. W.: The influence of particle composition and particle flux on scavenging of Th , Pa and Be in the ocean, Earth Planet. Sci. Lett., 204(1-2), 215–229, doi:10.1016/S0012-821X(02)00984-6, 2002.
Colley, S., Thomson, J. and Newton, P. P.: Detailed Th-230, Th-232 and Pb-210 fluxes recorded by the 1989/90 BOFS sediment trap time-series at 48 degrees N, 20 degrees W, Deep - Sea Res. Part I - Oceanogr. Res. Pap., 42(6), 833–848, 1995.
Danabasoglu, G., Bates, S. C., Briegleb, B. P., Jayne, S. R., Jochum, M., Large, W. G., Peacock, S. and Yeager, S. G.: The CCSM4 ocean component, J. Clim., 25(5), 1361–1389, doi:10.1175/JCLI-D-11-00091.1, 2012.

Doney, S. C., Lima, I., Feely, R. A., Glover, D. M., Lindsay, K., Mahowald, N., Moore, J. K.

Geoscientific Model Development Discussions

and Wanninkhof, R.: Mechanisms governing interannual variability in upper-ocean inorganic carbon system and air-sea CO2 fluxes: Physical climate and atmospheric dust, Deep. Res. Part II Top. Stud. Oceanogr., 56(8-10), 640–655, doi:10.1016/j.dsr2.2008.12.006, 2009.

Dutay, J.-C., Lacan, F., Roy-Barman, M. and Bopp, L.: Influence of particle size and type on 231 Pa and 230 Th simulation with a global coupled biogeochemical-ocean general circulation model: A first approach, Geochemistry, Geophys. Geosystems, 10(1), doi:10.1029/2008GC002291, 2009.

Francois, R., Bacon, M. P., Altabet, M. A. and Labeyrie, L. D.: Glacial/interglacial changes in sediment rain rate in the SW Indian Sector of subantarctic Waters as recorded by 230Th, 231Pa, U, and d15N, Paleoceanography, 8(5), 611–629, doi:10.1029/93PA00784, 1993.

Frank, M.: Reconstruction of Late Quaternary environmental conditions applying the natural radionuclides 230Th, 10Be, 231Pa and 238U: A study of deep-sea sediments from the eastern sector of the Antarctic Circumpolar Current System, Alfred Wegener Institute for Polar and Marine Research., 1996.

Frank, M., Eisenhauer, A., Kubik, P. W., Dittrich-hannen, B. and Segl, M.: Beryllium 10, thorium 230, and protactinium 231 in Galapagos microplate sediments: Implications of hydrothermal activity and paleoproductivity changes during the last 100,000 years, Palaeogeography, 9(4), 559–578, 1994.

Geibert, W. and Usbeck, R.: Adsorption of thorium and protactinium onto different particle types: Experimental findings, Geochim. Cosmochim. Acta, 68(7), 1489–1501, doi:10.1016/j.gca.2003.10.011, 2004.

Gherardi, J.-M., Labeyrie, L., Nave, S., Francois, R., McManus, J. F. and Cortijo, E.: Glacial-interglacial circulation changes inferred from 231 Pa/ 230 Th sedimentary record in the North Atlantic region, Paleoceanography, 24(2), doi:10.1029/2008PA001696, 2009.

Gu, S., Liu, Z., Jahn, A., Rempfer, J., Zhang, J., and Joos, F.: Neodymium isotopes in the ocean model of the Community Earth System Model (CESM1.3), Geosci. Model Dev. Discuss., doi:10.5194/gmd-2017-40, in review, 2017.

Henderson, G. M. and Anderson, R. F.: The U-series toolbox for paleoceanography, Rev. Mineral. Geochemistry, 52(1), 493–531, doi:10.2113/0520493, 2003.
Henderson, G. M., Heinze, C., Anderson, R. F. and Winguth, A. M. E.: Global distribution of the 230Th flux to ocean sediments constrained by GCM modelling, Deep. Res. Part I Oceanogr. Res. Pap., 46(11), 1861–1893, doi:10.1016/S0967-0637(99)00030-8, 1999.

Hurrell, J. W., Holland, M. M., Gent, P. R., Ghan, S., Kay, J. E., Kushner, P. J., Lamarque, J.

F., Large, W. G., Lawrence, D., Lindsay, K., Lipscomb, W. H., Long, M. C., Mahowald, N., Marsh, D. R., Neale, R. B., Rasch, P., Vavrus, S., Vertenstein, M., Bader, D., Collins, W. D., Hack, J. J., Kiehl, J. and Marshall, S.: The community earth system model: A framework for collaborative research, Bull. Am. Meteorol. Soc., 94(9), 1339–1360, doi:10.1175/BAMS-D-12-00121.1, 2013.

Jahn, A., Lindsay, K., Giraud, X., Gruber, N., Otto-Bliesner, B. L., Liu, Z. and Brady, E. C.: Carbon isotopes in the ocean model of the Community Earth System Model (CESM1), Geosci. Model Dev., 8(8), 2419–2434, doi:10.5194/gmd-8-2419-2015, 2015.

Keigwin, L. D. and Boyle, E. A.: Did North Atlantic overturning halt 17,000 years ago?, Paleoceanography, 23(1), 1–5, doi:10.1029/2007PA001500, 2008.
Kriest, I.: Different parameterizations of marine snow in a 1D-model and their influence on representation of marine snow, nitrogen budget and sedimentation, Deep. Res. Part I Oceanogr. Res. Pap., 49(12), 2133–2162, doi:10.1016/S0967-0637(02)00127-9, 2002.

Ku, T. L., Bischoff, J. L. and Boersma, A.: Age studies of Mid-Atlantic Ridge sediments near 42??N and 20??N, Deep. Res. Oceanogr. Abstr., 19(3), 233–247, doi:10.1016/0011-7471(72)90033-2, 1972.

Kumar, N., Gwiazda, R., Anderson, R. F. and Froelich, P. N.: 231Pa/230Th ratios in sediments as a proxy for past changes in Southern Ocean productivity, Nature, 362, 45–48, doi:10.1038/362045a0, 1993.

Large, W. G. and Yeager, S. G.: The global climatology of an interannually varying air–sea flux data set, Clim. Dyn., 33(2-3), 341–364, doi:10.1007/s00382-008-0441-3, 2008.

Lippold, J., Grützner, J., Winter, D., Lahaye, Y., Mangini, A. and Christi, M.: Does sedimentary 231Pa/230Th from the Bermuda Rise monitor past Atlantic Meridional Overturning Circulation?, Geophys. Res. Lett., 36(12), 1–6, doi:10.1029/2009GL038068, 2009.

Long, M. C., Lindsay, K., Peacock, S., Moore, J. K. and Doney, S. C.: Twentieth-century oceanic carbon uptake and storage in CESM1(BGC), J. Clim., 26(18), 6775–6800, doi:10.1175/JCLI-D-12-00184.s1, 2013.

Luo, C., Mahowald, N. and Corral, J.: Sensitivity study of meteorological parameters on mineral aerosol mobilization, transport, and distribution, J. Geophys. Res., 108(D15), 4447, doi:10.1029/2003JD003483, 2003.

Luo, S. and Ku, T. L.: Oceanic 231Pa/230Th ratio influenced by particle composition and remineralization, Earth Planet. Sci. Lett., 167(3-4), 183–195, doi:10.1016/S0012-821X(99)00035-7, 1999.

Luo, Y., Francois, R. and Allen, S.: Sediment 231Pa/230Th as a recorder of the rate of the Atlantic meridional overturning circulation: insights from a 2-D model, Ocean Sci., 6(3), 381–400, doi:10.5194/os-6-381-2010, 2010.

Mangini, A. and Key, R. M.: A 230Th profile in the Atlantic Ocean, Earth Planet. Sci. Lett., 62(3), 377–384, doi:10.1016/0012-821X(83)90008-0, 1983.

Marchal, O., François, R., Stocker, T. and Joos, F.: Ocean thermohaline circulation and sedimentary 231Pa/230Th ratio, Paleoceanography, 15(6), 625–641 [online] Available from: http://onlinelibrary.wiley.com/doi/10.1029/2000PA000496/full (Accessed 19 April 2016), 2000.

McManus, J., Francois, R. and Gherardi, J.: Collapse and rapid resumption of Atlantic meridional circulation linked to deglacial climate changes, Nature, 428(6985), 834–837, 2004.

Moore, J. K. and Braucher, O.: Sedimentary and mineral dust sources of dissolved iron to the World Ocean, Biogeosciences, 5(1994), 631–656, doi:10.5194/bgd-4-1279-2007, 2008.

Moore, J. K., Doney, S. C., Glover, D. M. and Fung, I. Y.: Iron cycling and nutrient-limitation patterns in surface waters of the World Ocean, , 49, 463–507, 2002.
Moore, J. K., Doney, S. C. and Lindsay, K.: Upper ocean ecosystem dynamics and iron cycling in a global three-dimensional model, Global Biogeochem. Cycles, 18(4), doi:10.1029/2004GB002220, 2004.

Moore, J. K., Lindsay, K., Doney, S. C., Long, M. C. and Misumi, K.: Marine Ecosystem Dynamics and Biogeochemical Cycling in the Community Earth System Model [CESM1(BGC)]: Comparison of the 1990s with the 2090s under the RCP4.5 and RCP8.5 Scenarios, J. Clim., 26(23), 9291–9312, doi:10.1175/JCLI-D-12-00566.1, 2013.

Moore, R. M. and Hunter, K. A.: Thorium adsorption in the ocean: reversibility and distribution amongst particle sizes, Geochim. Cosmochim. Acta, 49(11), 2253–2257, doi:10.1016/0016-7037(85)90225-X, 1985.

Moran, S. B., Charette, M. a., Hoff, J. a., Edwards, R. L. and Landing, W. M.: Distribution of 230Th in the Labrador Sea and its relation to ventilation, Earth Planet. Sci. Lett., 150, 151–160, doi:10.1016/S0012-821X(97)00081-2, 1997.

Moran, S. B., Shen, C. C., Edmonds, H. N., Weinstein, S. E., Smith, J. N. and Edwards, R. L.: Dissolved and particulate 231Pa and 230Th in the Atlantic Ocean: Constraints on intermediate/deep water age, boundary scavenging, and 231Pa/230Th fractionation, Earth Planet. Sci. Lett., 203(3-4), 999–1014, doi:10.1016/S0012-821X(02)00928-7, 2002.

Müller, P. J. and Mangini, A.: Organic carbon decomposition rates in sediments of the pacific manganese nodule belt dated by 230Th and 231Pa, Earth Planet. Sci. Lett., 51(1), 94–114, doi:10.1016/0012-821X(80)90259-9, 1980.

Nozaki, Y., Yang, H.-S. and Yamada, M.: Scavenging of thorium in the ocean, J. Geophys. Res., 92(C1), 772, doi:10.1029/JC092iC01p00772, 1987.

Roy-Barman, M., Chen, J. H. and Wasserburg, G. J.: 230Th-232Th systematics in the central Pacific Ocean: The sources and the fates of thorium, Earth Planet. Sci. Lett., 139(3-4), 351–363, doi:10.1016/0012-821X(96)00017-9, 1996.

Rutgers van der Loeff, M. M. and Berger, G. W.: Scavenging of 230Th and 231Pa near the antarctic polar front in the South Atlantic, Deep. Res. Part I, 40(2), 339–357, doi:10.1016/0967-0637(93)90007-P, 1993.

Schmittner, A.: Decline of the marine ecosystem caused by a reduction in the Atlantic overturning circulation., Nature, 434(7033), 628–633, doi:10.1038/nature03476, 2005.

Schmitz, W., Mangini, A., Stoffers, P., Glasby, G. P. and Pluger, W. L.: Sediment accumulation rates in the southwestern Pacific Basin and Aitutaki Passage, Mar. Geol., 73(1), 181–190, 1986.

Scholten, J. C., Rutgers van der Loeff, M. M. and Michel, A.: Distribution of 230Th and 231Pa in the water column in relation to the ventilation of the deep Arctic basins, Deep. Res. Part II, 42(6), 1519–1531, doi:10.1016/0967-0645(95)00052-6, 1995.

Scholten, J. C., Fietzke, J., Mangini, A., Garbe-Schönberg, C. D., Eisenhauer, A., Schneider, R. and Stoffers, P.: Advection and scavenging: Effects on 230Th and 231Pa distribution off Southwest Africa, Earth Planet. Sci. Lett., 271(1-4), 159–169, doi:10.1016/j.epsl.2008.03.060, 2008.

Shimmield, G. B. and Price, N. B.: The scavenging of U,230Th and 231Pa during pulsed hydrothermal activity at 20??S, East Pacific Rise, Geochim. Cosmochim. Acta, 52(3), 669–677, doi:10.1016/0016-7037(88)90329-8, 1988.

Shimmield, G. B., Murray, J. W., Thomson, J., Bacon, M. P., Anderson, R. F. and Price, N. B.: The distribution and behaviour of 230Th and 231Pa at an ocean margin, Baja California, Mexico, Geochim. Cosmochim. Acta, 50(11), 2499–2507, doi:10.1016/0016-7037(86)90032-3, 1986.

Siddall, M., Henderson, G. M., Edwards, N. R., Frank, M., Müller, S. a., Stocker, T. F. and Joos, F.: 231Pa/230Th fractionation by ocean transport, biogenic particle flux and particle type, Earth Planet. Sci. Lett., 237(1-2), 135–155, doi:10.1016/j.epsl.2005.05.031, 2005.

Geosci. Model Dev. Discuss., doi:10.5194/gmd-2017-82, 2017
Manuscript under review for journal Geosci. Model Dev.
Discussion started: 20 April 2017

Siddall, M., Stocker, T. F., Henderson, G. M., Joos, F., Frank, M., Edwards, N. R., Ritz, S. P. and Müller, S. a.: Modeling the relationship between 231 Pa/ 230 Th distribution in North Atlantic sediment and Atlantic meridional overturning circulation, Paleoceanography, 22(2), doi:10.1029/2006PA001358, 2007.

Thomas, A. L., Henderson, G. M. and Robinson, L. F.: Interpretation of the 231Pa/230Th paleocirculation proxy: New water-column measurements from the southwest Indian Ocean, Earth Planet. Sci. Lett., 241(3-4), 493–504, doi:10.1016/j.epsl.2005.11.031, 2006.

VOGLER, S., SCHOLTEN, J., RUTGERSVANDERLOEFF, M. and MANGINI, A.: 230Th in the eastern North Atlantic: the importance of water mass ventilation in the balance of230Th, Earth Planet. Sci. Lett., 156(1-2), 61–74, doi:10.1016/S0012-821X(98)00011-9, 1998.

Walter, H. J., Rutgers van der Loeff, M. M. and Hoeltzen, H.: Enhanced scavenging of 231Pa relative to 230Th in the South Atlantic south of the Polar Front: Implications for the use of the 231Pa/230Th ratio as a paleoproductivity proxy, Earth Planet. Sci. Lett., 149(1), 85–100, doi:10.1016/S0012-821X(97)00068-X, 1997.

Yang, H. S., Nozaki, Y., Sakai, H. and Masuda, A.: The distribution of 230Th and 231Pa in the deep-sea surface sediments of the Pacific Ocean, Geochim. Cosmochim. Acta, 50(1), 81–89, doi:10.1016/0016-7037(86)90050-5, 1986.

Yong Lao, Anderson, R. F., Broecker, W. S., Trumbore, S. E., Hofmann, H. J. and Wolfli, W.: Transport and burial rates of 10Be and 231Pa in the Pacific Ocean during the Holocene period, Earth Planet. Sci. Lett., 113(1-2), 173–189, doi:10.1016/0012-821X(92)90218-K, 1992.

Yong-Liang Yang, Elderfield, H., Pedersen, T. F. and Ivanovich, M.: Geochemical record of the Panama Basin during the Last Glacial Maximum carbon event shows that the glacial ocean was not suboxic, Geology, 23(12), 1115–1118, doi:10.1130/0091-7613(1995)023<1115:GROTPB>2.3.CO, 1995.

Yu, E.-F., Francois, R. and Bacon, M. P.: Similar rates of modern and last-glacial ocean thermohaline circulation inferred from radiochemical data, Nature, 379(6567), 689–694, doi:10.1038/379689a0, 1996.

	CTRL		EXP_1		EXP_2	
	^{231}Pa	^{230}Th	^{231}Pa	^{230}Th	^{231}Pa	^{230}Th
K_{CaCO_3}	2.5*10^5	1.0*10^7	5*10^4	2*10^6	1.25*10^6	5*10^7
K_{opal}	1.67*10^6	5*10^5	3.33*10^5	1*10^5	8.33*10^6	2.5*10^6
K_{POC}	1.0*10^7	1.0*10^7	2*10^6	2*10^6	5*10^7	5*10^7
K_{dust}	0	0	0	0	0	0
T(yr)	118	33	501	143	27	9

Table 1. Partition coefficients for different particle types and residence time for ^{231}Pa and ^{230}Th in different experiments.

Geoscientific Model Development Discussions Open Access EGU

Figures:

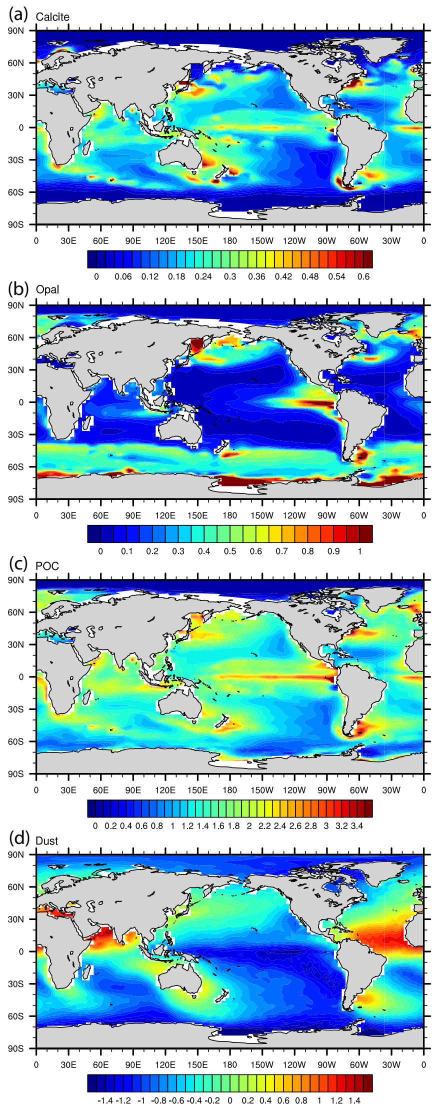

Figure 1. Annual mean particle fluxes in CESM. (a) $CaCO_3$ flux at 105m (mol m^{-2} yr^{-1}). (b) Opal flux at 105m (mol m^{-2} yr^{-1}). (c) POC flux at 105m (mol m^{-2} yr^{-1}). (d) Log10 values of annual atmospheric dust deposition (g m^{-2} yr^{-1}).

Geosci. Model Dev. Discuss., doi:10.5194/gmd-2017-82, 2017
Manuscript under review for journal Geosci. Model Dev.
Discussion started: 20 April 2017

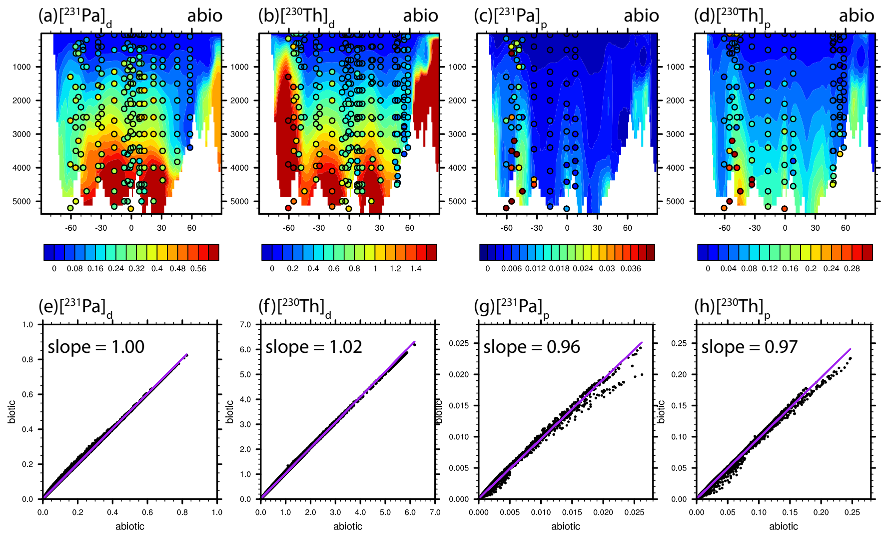

Figure 2. Atlantic zonal mean dissolved and particulate abiotic ^{231}Pa and ^{230}Th in CTRL (unit: dpm/m^3): (a) dissolved ^{231}Pa; (b) dissolved ^{230}Th; (c) particulate ^{231}Pa; (d) particulate ^{230}Th. Scatter plot of global dissolved and particulate ^{231}Pa and ^{230}Th between abiotic and biotic in CTRL: (e) dissolved ^{231}Pa; (f) dissolved ^{230}Th; (g) particulate ^{231}Pa; (h) particulate ^{230}Th. Purple line is the least squared linear regression line and slope is the linear regression coefficient.

Geosci. Model Dev. Discuss., doi:10.5194/gmd-2017-82, 2017
Manuscript under review for journal Geosci. Model Dev.
Discussion started: 20 April 2017

Geoscientific Model Development
Discussions
Open Access

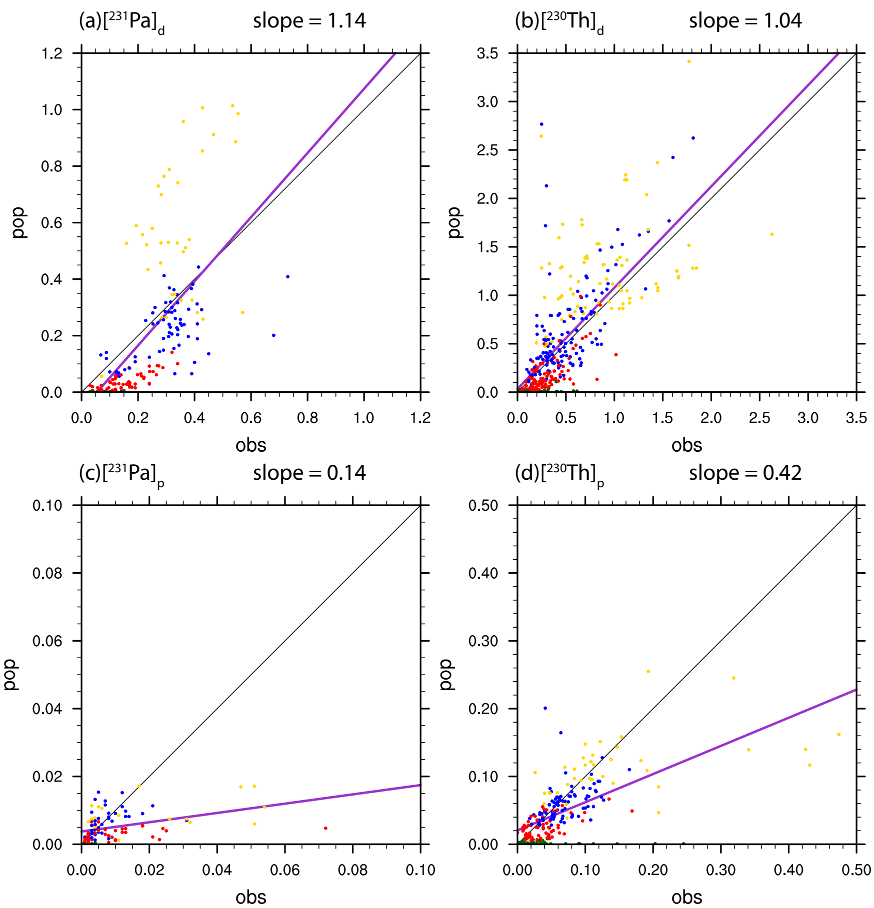

Figure 3. Scatter plot of global dissolved and particulate ^{231}Pa and ^{230}Th between observation and CTRL (abiotic) (unit: dpm/m^3). (a) dissolved ^{231}Pa; (b) particulate ^{231}Pa; (c) dissolved ^{230}Th; (d) particulate ^{230}Th. Observations in different depth range are indicated by different colors: green for 0-100m; red for 100m-1000m; blue for 1000m-3000m and yellow for deeper than 3000m. Purple line is the least squared linear regression line and slope is the linear regression coefficient.

Geosci. Model Dev. Discuss., doi:10.5194/gmd-2017-82, 2017
Manuscript under review for journal Geosci. Model Dev.
Discussion started: 20 April 2017

Geoscientific Model Development Discussions
Open Access
EGU

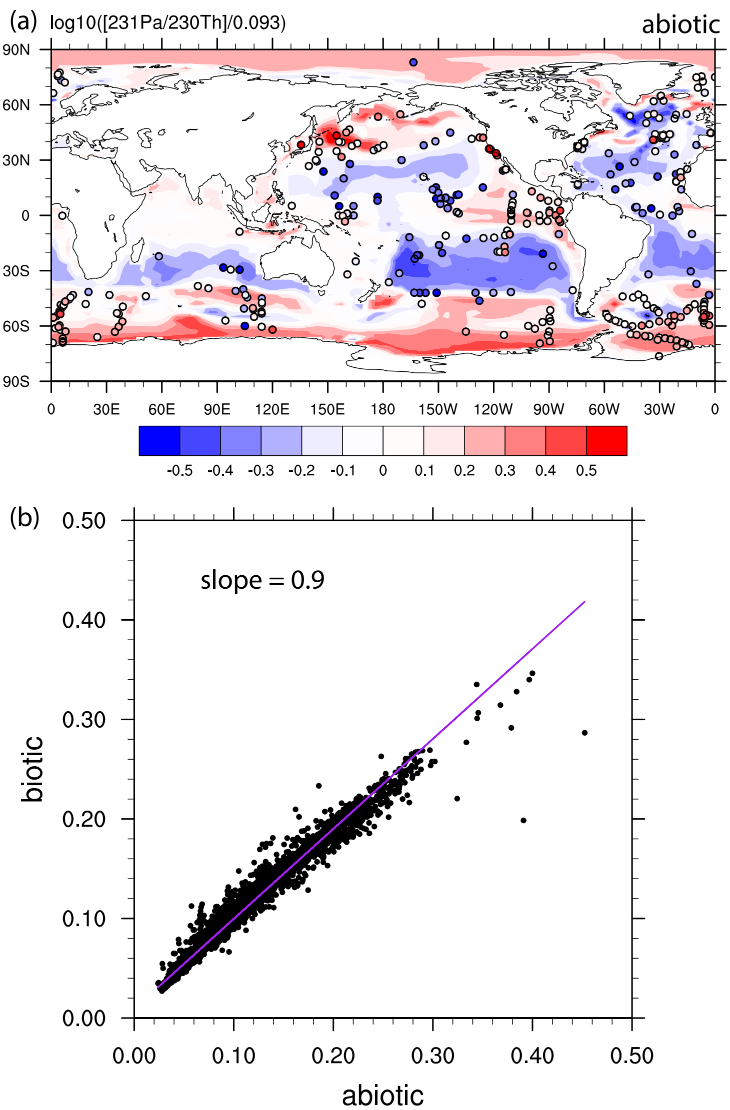

Figure 4. (a) Abiotic sediment $^{231}Pa/^{230}Th$ activity ratio in CTRL Observations are attached as filled cycles using the same color map. The $^{231}Pa/^{230}Th$ activity ratio is plotted relative to the production ratio of 0.093 on a $\log_{10}$ scale. (b) Scatter plot of abiotic and biotic sediment $^{231}Pa/^{230}Th$ activity ratio in CTRL. Purple line is the least squared linear regression line and slope is the linear regression coefficient.

Geosci. Model Dev. Discuss., doi:10.5194/gmd-2017-82, 2017
Manuscript under review for journal Geosci. Model Dev.
Discussion started: 20 April 2017

Geoscientific Model Development
Discussions
Open Access

Sediment ^{231}Pa/^{230}Th activity ratio is calculated using $[^{231}Pa]_p/[^{230}Th]_p$ is the bottom grid box in the model.

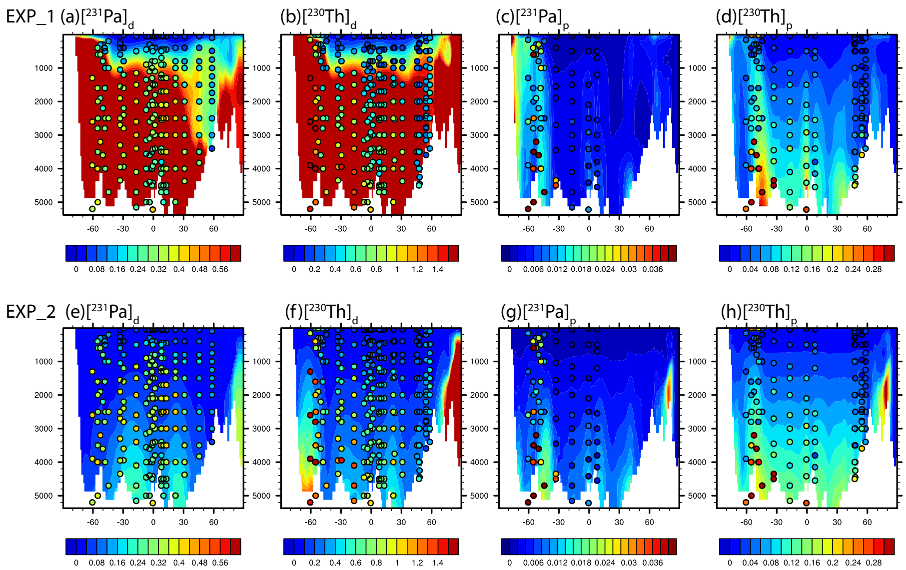

Figure 5. Atlantic zonal mean dissolved and particulate ^{231}Pa and ^{230}Th in EXP_1 and EXP_2 (unit: dpm/m^3). EXP_1: (a) dissolved ^{231}Pa; (b) dissolved ^{230}Th; (c) particulate ^{231}Pa; (d) particulate ^{230}Th. EXP_2: (e) dissolved ^{231}Pa; (f) dissolved ^{230}Th; (g) particulate ^{231}Pa; (h) particulate ^{230}Th. Observations are attached as filled cycles using the same color map.

Geosci. Model Dev. Discuss., doi:10.5194/gmd-2017-82, 2017
Manuscript under review for journal Geosci. Model Dev.
Discussion started: 20 April 2017

Geoscientific Model Development Discussions
Open Access

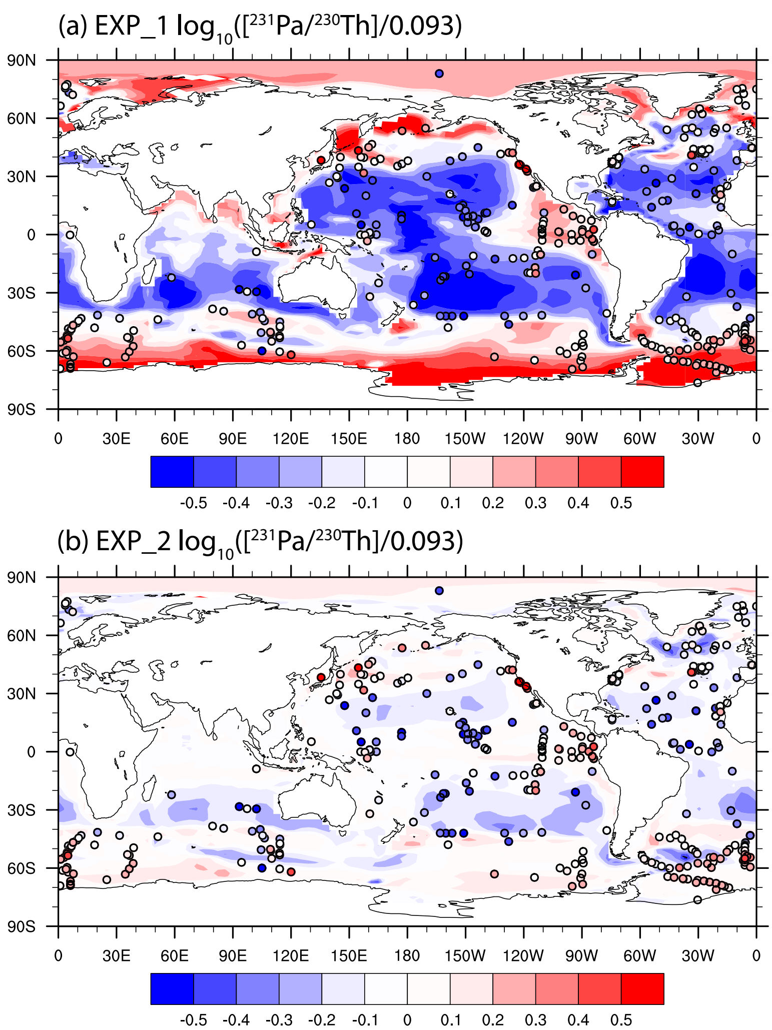

Figure 6. Sediment $^{231}Pa/^{230}Th$ activity ratio in EXP_1 (a) and EXP_2 (b). Observations are attached as filled cycles using the same color map. The $^{231}Pa/^{230}Th$ activity ratio is plotted relative to the production ratio of 0.093 on a $\log_{10}$ scale.

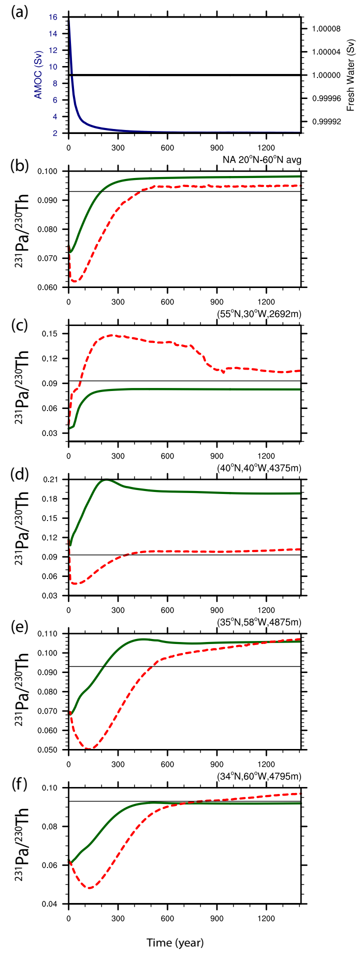

Figure 7. Time evolutions in HOSING. (a) Freshwater forcing (black) and AMOC strength (navy), which is defined as the maximum of the overturning streamfunction below 500m in the North Atlantic. (b) North Atlantic average sediment $^{231}Pa/^{230}Th$ activity ratio from 20°N to 60°N: abiotic (green) and biotic (red). Production ratio of 0.093 is indicated by a solid black line (similar in c, d, e and f). (c) Sediment $^{231}Pa/^{230}Th$ activity ratio at (55°N, 30°W). (d) Sediment $^{231}Pa/^{230}Th$ activity ratio at (40°N, 40°W). (e) Sediment $^{231}Pa/^{230}Th$ activity ratio at (35°N, 58°W). (f) Sediment $^{231}Pa/^{230}Th$ activity ratio at (34°N, 60°W). (e) and (f) are near Bermuda Rise. Locations of each site are shown as dots in Fig. 8b.

Geosci. Model Dev. Discuss., doi:10.5194/gmd-2017-82, 2017
Manuscript under review for journal Geosci. Model Dev.
Discussion started: 20 April 2017

Geoscientific Model Development Discussions

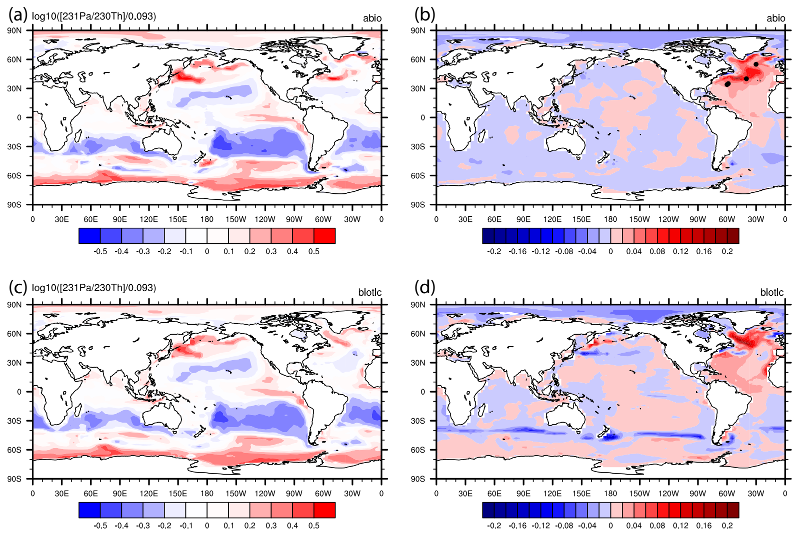

Figure 8. Sediment $^{231}Pa/^{230}Th$ activity ratio during AMOC off state and the difference between AMOC off and CTRL. (a) Abiotic $\log_{10}([^{231}Pa/^{230}Th]/0.093)$ in AMOC_off. (b) Difference of abiotic sediment $^{231}Pa/^{230}Th$ activity ratio between AMOC_off and AMOC_on. (c) and (d) are similar to (a) and (b) for biotic sediment $^{231}Pa/^{230}Th$ activity ratio. Black dots in (b) shows the locations of sites in Fig. 7 from North to South.

Geosci. Model Dev. Discuss., doi:10.5194/gmd-2017-82, 2017
Manuscript under review for journal Geosci. Model Dev.
Discussion started: 20 April 2017

Geoscientific Model Development Discussions

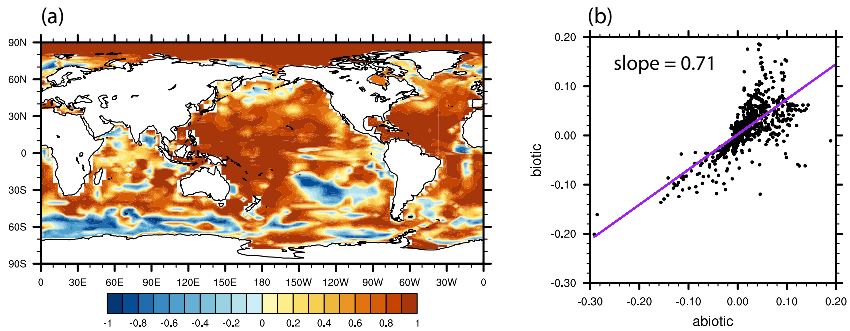

Figure 9. (a) Correlation of abiotic and biotic evolution of sediment $^{231}Pa/^{230}Th$ activity ratio in HOSING. (b) Scatter plot of abiotic and biotic sediment $^{231}Pa/^{230}Th$ activity ratio change from AMOC_on to AMOC_off in the Atlantic and the Southern Ocean (70°W-20°E). Purple line is the least squared linear regression line and slope is the linear regression coefficient.